International Journal of Nanomedicine

Dovepress
open access to scientific and medical research

Open Access Full Text Article

ORIGINAL RESEARCH

# Oriented Graphene Oxide Scaffold Promotes Nerve Regeneration in vitro and in vivo

Xu Zhou[1,2,*], Aolin Tang[2,3,*], Chengjie Xiong[2,*], Guoquan Zhang[2], Liangliang Huang[1,2], Feng Xu[1,2]

[1]The First School of Clinical Medicine, Southern Medical University, Guangzhou, 510515, People's Republic of China; [2]Department of Orthopaedics, General Hospital of Central Theater Command, Wuhan, 430070, People's Republic of China; [3]Department of Orthopaedics, Minda Hospital of Hubei Minzu University, Enshi, 445000, People's Republic of China

*These authors contributed equally to this work

Correspondence: Liangliang Huang; Feng Xu, Department of Orthopaedics, General Hospital of Central Theater Command, Wuhan, 430070, People's Republic of China, Email hll666789@163.com; fengxu1969@163.com



**Background:** Treating peripheral nerve injuries (PNI) with defects remains challenging in clinical practice. The commercial conduits have shown suboptimal nerve regeneration and functional recovery due to their basic tubular design without electroactive and oriented topographical cues.

**Purpose:** To develop a new scaffold with oriented microstructure and electroactive Graphene oxide (GO) and investigate its' therapeutic effect on nerve regeneration in vitro and in vivo.

**Methods:** This study employed a straightforward approach to co-spin PCL and GO, yielding an oriented hybrid nanofibrous scaffold known as the O-GO/PCL scaffold. The physical and chemical properties of nanofibrous scaffold were tested by scanning electron microscopy (SEM), transmission electron microscope (TEM), tensile test and so on. Primary Schwann cells (SCs) and dorsal root ganglia (DRG) were used to investigate the impact of the newly developed scaffolds on the biological behavior of neural cells in vitro. Transcriptome sequencing (mRNA-seq) was employed to probe the underlying mechanisms of the synergistic effect of electroactive GO and longitudinal topographic guidance on nerve regeneration. Furthermore, the developed O-GO/PCL scaffold was utilized to bridge a 10-mm sciatic nerve defect in rat, aiming to investigate its therapeutic potential for peripheral nerve regeneration in vivo.

**Results and discussion:** The SEM and TEM revealed that the newly developed O-GO/PCL scaffold showed longitudinally oriented microstructure and GO particles were homogenously and uniformly distributed inside the nanofibers. Primary SCs were utilized to assess the biocompatibility of the GO-based scaffold, revealing that negligible cytotoxicity when GO concentration does not exceed 0.5%. In vitro analysis of nerve regeneration demonstrated that axons in the O-GO/PCL group exhibited an average length of 1054.88 ± 161.32 μm, significant longer than those in the other groups ($P < 0.05$). Moreover, mRNA sequencing results suggested that the O-GO/PCL scaffold could enhance nerve regeneration by upregulating genes associated with neural regeneration, encompassing ion transport, axon guidance and cell–cell interactions. Most importantly, we employed the O-GO/PCL scaffold to repair a 10-mm sciatic nerve defect in rat, resulting in augmented nerve regeneration, myelination, and functional recovery.

**Conclusion:** The O-GO/PCL scaffold with oriented microstructure and electroactive GO represents a promising heral nerve reconstruction.

**Keywords:** nanofibers, topographical guidance, electroactive, graphene oxide, nerve regeneration

## Introduction

Peripheral nerve injury represents a prevalent global health issue, impacting over 5 million individuals worldwide.[1,2] Despite significant advancements in microsurgical techniques in recent years, effectively addressing nerve defects remains a formidable challenge. While autografts have stood as the gold standard for nerve defect repair, they are plagued by issues like donor nerve scarcity, secondary trauma, and neuroma formation.[3] In recent years, artificial nerve conduits, including NeuroTube, NeuraGen, NeuroMatrix, and others, have been developed as an alternative approach.[4] However, these commercial conduits have shown

Received: 24 October 2023
Accepted: 14 February 2024
Published: 13 March 2024

**Graphical Abstract**

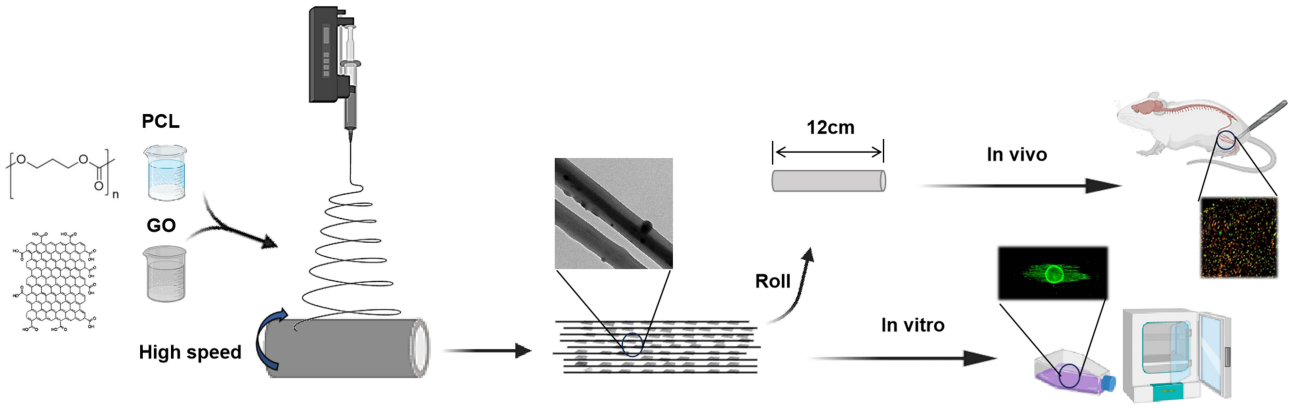


suboptimal nerve regeneration and functional recovery due to their basic tubular design that offers only general guidance.[5,6] Consequently, there is a pressing need for innovative solutions with enhanced effectiveness for nerve repair in clinical scenarios.

It is now understood that following peripheral nervous system (PNS) injuries, the distal nerve stump undergoes Wallerian degeneration and forms aligned Büngner bands, facilitating and promoting axon growth. Inspired by the organized structures of the PNS, longitudinal microstructures such as aligned fibers, microgrooves, and microchannels have been introduced into nerve guidance scaffolds (NGSs) using various methods like electrospinning, phase separation, microstereolithography, template thermo-crosslinking, and mold freeze-drying.[7–11] Electrospinning offers numerous advantages, including ease of use, customizable scaffold structure, adjustable fiber diameter, and suitability for various materials. State-of-the-art techniques have enabled the production of highly aligned fibers that mimic tissue structures, thereby improving regeneration.[12,13] For instance, Wang et al demonstrated that highly aligned electrospun poly-L-lactic acid (PLLA) fibers with appropriate diameters encouraged neurite extension and Schwann cell (SC) migration.[14] Besides, Zhang et al reported that aligned nanofibers offered optimal topographical cues for guiding cell and neurite growth in specific orientations.[15]

Beyond topographical cues defined by the scaffold's microstructure, the significance of electroactive functional materials has gained prominence.[16–18] Among these conductive materials, graphene oxide (GO) stands out due to its exceptional electrical conductivity, biocompatibility, and favorable interactions with cell interfaces. The negative carboxylate groups on GO enhance colloidal stability and hydrophilicity, making it suitable for surface attachment, proliferation, and differentiation of nerve cells.[19] Li et al demonstrated that GO significantly stimulates neural cell proliferation and differentiation.[20] Importantly, SCs exhibited improved adhesion, proliferation, and neurotrophic factor secretion on GO-based substrates. GO has also been shown to enhance neuro-specific gene expression, neurite outgrowth, and sprouting in neuronal-like cells.[21]

Recently, a significant amount of effort has been taken in developing nerve scaffolds with oriented microstructures and electroactive GO to promote nerve regeneration. Most of these strategies have successfully coated GO onto 2D surfaces. However, the coated GO is easy to detach from the 2D surfaces. Thus, it is challenging to translate them into 3D implantable scaffolds for clinical use.[15,22] Furthermore, most of these studies have just investigated the effect of oriented microstructures and electroactive GO on nerve regeneration using cell lines (such as PC12 and RSC96) in vitro. Notably, the cell lines are tumor-like cells, which show different biological characteristics compared with primary cells and in vivo situations. Moreover, the mechanisms underlying the synergistic impact of electroactive GO and oriented topographic guidance on nerve regeneration remains largely unexplored. Thus, for potential clinical applications, it is imperative to adopt a more straightforward approach to fabricate nerve scaffolds with electroactive GO and oriented microstructures topography, assess the therapeutic effect of the scaffolds using primary cell cultures and in vivo animal models, and comprehend the underlying mechanisms.

In the present study, we employed a straightforward technique to co-spin polycaprolactone (PCL) and GO, resulting in an oriented GO/PCL hybrid nanofibrous scaffold termed the O-GO/PCL scaffold. The physical and chemical properties of nanofibrous scaffold were tested by scanning electron microscopy (SEM), transmission electron microscope (TEM), tensile

properties, 4-point probe method, Fourier transform infrared (FTIR), and contact angle analysis. The impact of these developed scaffolds on the biological properties and behavior of neural cells was examined through co-culturing with primary SCs and dorsal root ganglia (DRG) in vitro. Transcriptome sequencing (mRNA-seq) was employed to probe the underlying mechanisms of the synergistic effect of electroactive GO and longitudinal topographic guidance on nerve regeneration. Furthermore, the developed O-GO/PCL NGS was utilized to bridge a 10 mm sciatic nerve defect in rats, aiming to investigate its therapeutic potential for peripheral nerve regeneration in vivo.

## Materials and Methods

### Fabrication of GO/PCL Scaffold

An electrospinning technique was employed to create electrospun scaffolds in random and aligned orientations. In a brief overview, as illustrated in Figure 1, GO powder was dispersed in 1,1,1,3,3,3-hexafluoro-2-propanol (HFIP) and sonicated at 80 Hz for 2 hours in a temperature-controlled (room temperature) ultrasonic bath to produce a GO dispersion. Following sonication, PCL was added to the GO dispersion and stirred for 24 hours at room temperature. Solutions with varying concentrations of GO/PCL were prepared, increasing the GO loading to 0.1%, 0.3%, 0.5%, and 1.0% by weight.

Electrospinning was conducted with a high voltage of 12 kV at a flow rate of 2 mL/hour. Aligned fibers were collected on a high-speed (2800 rpm) collecting drum with tin foil, maintaining a 15 cm distance from the spinneret. Random fibers were collected on a slow-speed (120 rpm) collecting drum with tin foil. All collected tin foil fibers were freeze-dried for 24 hours and stored at −20°C. The oriented and random GO/PCL nanofibrous scaffolds were denoted as O-GO/PCL and R-GO/PCL,

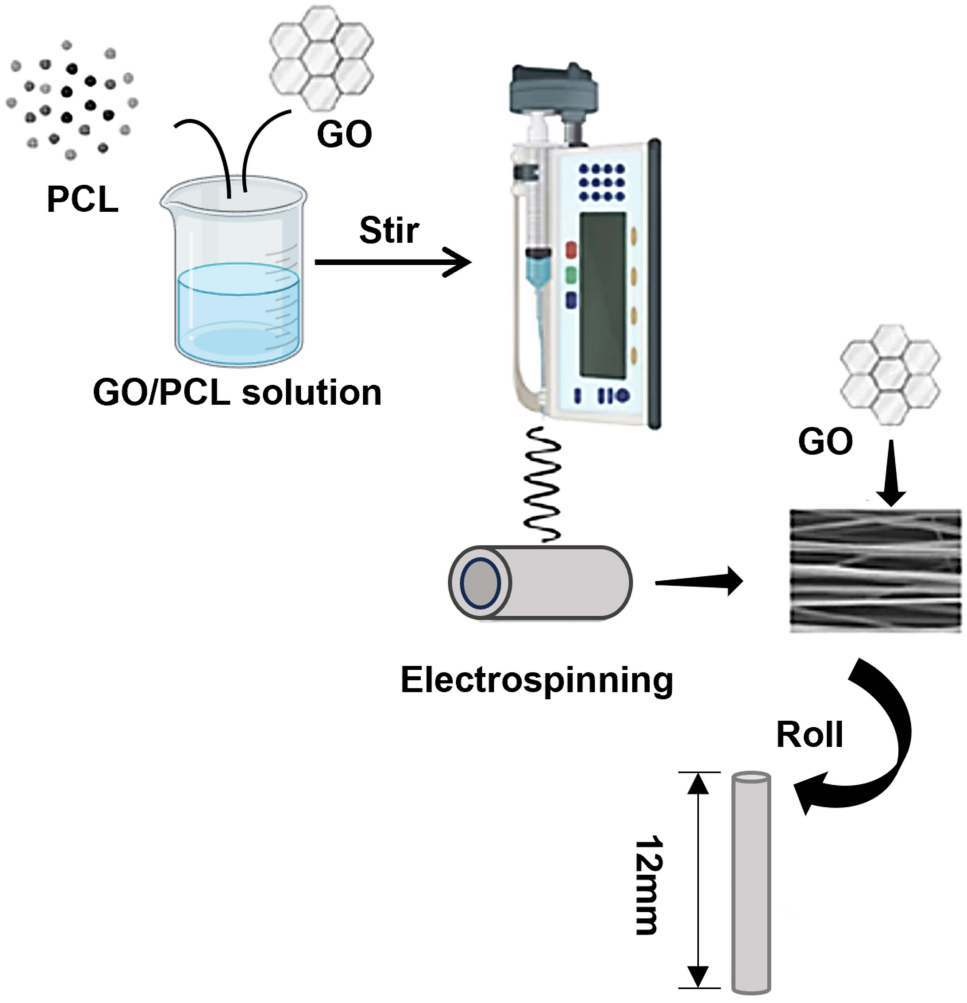


**Figure 1** Schematic diagrams of the fabrication of O-GO/PCL fiber scaffolds.

respectively. For the in vivo nerve regeneration study, 3D NGS were created by rolling R-PCL, O-PCL, R-GO/PCL, and O-GO/PCL nanofibrous scaffolds onto cylindrical polytetrafluoroethylene (PTFE) rods.

## Characterization of GO/PCL Scaffold

The microstructure of the scaffolds were observed using SEM (SU8220, Hitachi, Japan). Prior to observation, the samples were gold sputter-coated at 10 mA. To observe the distribution of GO in PCL nanofibers, the scaffolds were imaged under TEM (HF-3300, Hitachi, Japan). The static water contact angle on the surface of the nanofibrous scaffolds was measured by a contact angle test system (JC2000C, Zhongchen, China). The contact angle was measured by adding 1 μL of ultrapure water droplets to the film. The physical properties of different nanofibrous scaffolds were tested by tensile properties. Tensile tests were tested by a universal testing machine (Instron + MTS) to evaluate the mechanical properties of the spun film doped with different GO contents. The conductivity of GO/PCL was measured by the 4-point probe method using the Hall effect testing system (HL5500PC, Accent Optical, UK). The infrared spectroscopy was performed over the 400–4000 $cm^{-1}$ range and a resolution of 2 $cm^{-1}$ to analyze the distinctive bonds of GO/PCL composites. The FTIR spectra of the GO/PCL scaffolds were recorded using an infrared spectrometer (Vertex 80V spectrometer, Bruker, Germany) within the 400–4000 $cm^{-1}$ range.

## Cells Live/Dead Cell Staining

To simulate potential cellular toxicity of the GO/PCL scaffold to in situ neural cells, primary SCs were utilized for biocompatibility testing instead of cell lines. Primary SCs were obtained by dissecting and digesting the sciatic nerve and brachial plexus nerve from neonatal rats (postnatal day 1) and undergoing passaging culture. GO/PCL scaffolds with varying GO concentrations (0.1%, 0.3%, 0.5%, 1.0%) were cut into 6 mm diameter discs using a puncher, sterilized with 75% ethanol for 2 hours, and then rinsed with 0.01 M PBS under ultraviolet light until the ethanol was completely removed (approximately 24 hours, 6 times). These scaffolds were placed onto 24-well plates and seeded with SCs at a density of $2 \times 10^4$ cells/mL (1 mL medium) in each well. The Live/Dead cell staining kit (Yeasen, China) was used for cell viability analysis according to the standard protocol. Calcein-AM and propidium iodide (PI) were prepared separately as 30 μM PBS solutions and added to cover the cells/scaffold completely. Following the removal of the working solution, the samples were washed with PBS three times and observed under an inverted fluorescence microscope.

## DRG Explant

For enhanced neurite growth and alignment visualization in vitro, DRGs from neonatal rats were dissected and digested with 0.125% trypsin (Servicebio, China) for 15 minutes. The DRGs were then placed on the surfaces of O-GO/PCL, R-GO/PCL, O-PCL, and R-PCL scaffolds. The cultures were maintained for 4 days in vitro, fixed with 4% paraformaldehyde, and incubated with rabbit anti-S100 monoclonal antibody (1:200; Abcam, UK) and mouse anti-β-tubulin III (1:200; Abcam, UK) at 4°C overnight. The primary antibodies were visualized using goat anti-mouse Alexa 488 (1:500; Servicebio, China) and goat anti-rabbit Alexa 594 (1:500; Servicebio, China). Stained sections were examined using a fluorescence microscope (H600L, Nikon, Japan) and recorded for analysis using Image J 1.8 software.

## mRNA Sequencing and Transcriptome Data Analysis

Scaffolds (3.4 cm in diameter) were placed in 6-well plates and PBS-washed three times. DRGs were seeded onto O-GO/PCL, R-GO/PCL, O-PCL, and R-PCL nanofiber scaffolds, as well as in 6-well plates (n = 3) at a density of $8 \times 10^5$ cells/well. Cells were grown in a DMEM medium for 48 hours. Total RNA was extracted from each group using TRIzol reagent (Ambion, USA) and subsequently sent to BGI Corporation (Shenzhen, China) for RNA-seq detection and analysis via BGISEQ sequencer. Pathway analysis for differentially expressed genes (DEGs) was performed based on the Kyoto Encyclopedia of Genes and Genomes (KEGG) and gene ontology databases. Data analysis was conducted on the Dr. Tom network platform of BGI (http://report.bgi.com) and a free online platform (bioinformatics.com.cn).

## Animal Surgery

A rat peripheral nerve defect model was employed to examine the nerve regeneration capacity of the scaffolds in vivo. All animal procedures were approved by the Institutional Ethical Committee of the General Hospital of Central Theater

Command (No. 2019008) and conducted in accordance with the National Institutes of Health guide for the care and use of Laboratory animals (NIH Publications No. 8023, revised 1978) in the Hubei Medical Laboratory Animal Center. Sterile 0.01 M PBS was used to immerse all scaffolds for 24 hours after UA irradiation to soften the conduits for surgical procedures. Adult male Sprague Dawley rats (200–220 g) were randomly allocated into five groups: O-GO/PCL, R-GO/PCL, O-PCL, R-PCL, and autograft groups (ANT). Anesthesia was induced using 40 mg/kg 1% sodium pentobarbital injected into the peritoneal cavity. The right sciatic nerves were exposed through a gluteal muscle incision, creating a 10-mm gap. Both proximal and distal ends were inserted 1 mm into 12 mm-long scaffolds and sutured using 9–0 nylon sutures. Subsequently, muscles and skin were sutured using 4–0 nylon sutures. Penicillin injection was administered intraperitoneally immediately after surgery, and animals were provided standard access to food and water throughout the study.

### Immunofluorescent Assay of Regenerated Nerves in vivo

At 12 weeks post-surgery, the middle segments of the grafts were isolated and fixed with 4% paraformaldehyde. Cross-sectional slices with a thickness of 10.0 μm were prepared using a cryosection system. These sections were immunostained using the mouse anti-myelin basic protein (MBP) antibody (1:200; Abcam, UK) and rabbit anti-NF200 antibody (1:200; Servicebio, China). Fluorescence images were captured using a fluorescence microscope (H600L, Nikon, Japan), and the regenerated axon area and MBP and NF200 positive area were quantified and merged using Image J 1.8 software.

### Morphogenesis of Regenerated Nerves

For morphological analysis, distal segments of regenerated nerves were fixed with 4 wt% glutaraldehyde and sliced into ultrathin sections. These sections were stained with toluidine blue and examined under a light microscope. Positively stained axons and myelin were analyzed using Image J 1.8 software. Axon diameter and myelin thickness of regenerated nerves were assessed using TEM (JEM-2100, JEOL, Japan) and calculated with Image J 1.8 software.

### Muscle Weight and Histological Analysis

At 12 weeks post-operation, the gastrocnemius muscles from both the injured and uninjured sides of the sacrificed animals were harvested and weighed to determine the wet weight ratio of muscles (wet weight of muscle on the injured side/wet weight of muscle on the uninjured side × 100%). The gastrocnemius muscles were then fixed in formalin solution for 1 week, embedded in paraffin, and subjected to Masson staining. The average cross-sectional areas of muscle fibers were measured from the sliced images using ImageJ 1.8 software.

### Footprint Analysis

Walking track analysis was conducted at 6 and 12 weeks post-surgery to assess functional recovery as described previously.[23] Hind paws of rats were coated with stain before walking on a white paper track. The sciatic functional index (SFI) was calculated using the formula: SFI = 109.5 (ETS - NTS)/NTS + 13.3 (EIT - DNIT)/NIT - 38.3 (EPL - NPL)/NPL - 8.8, where PL represents paw length, TS is toe-spread distance between toes 1 and 5, and IT is toe-spread between toes 2 and 4. Measurements were taken from the normal (N) and experimental (E) sides.

### Statistical Analysis

Data were presented as mean ± standard deviation (SD). Statistical differences were analyzed using one-way analysis of variance (ANOVA) with the Tukey post-hoc method in GraphPad Prism 8 software. The level of significance was set at $p < 0.05$.

## Results

### Preparation and Characterization of O-GO/PCL Scaffold

A straightforward technique to fabricate O-GO/PCL scaffolds, featuring a uniform longitudinally oriented microstructure with incorporated electroactive GO, is illustrated in Figure 1. After ultrasonic mixing of GO and PCL, GO was evenly dispersed in the

PCL solution. The color of the GO/PCL scaffold darkened with increasing GO concentration (Supplemental Figure 1A–E). SEM analysis revealed a longitudinally oriented microstructure in the O-GO/PCL scaffold (Figure 2A and B), while no distinct orientation was observed in the R-GO/PCL scaffold (Figure 2D and E). Using the longitudinal axis of the conduits as the reference direction, fibers in R-GO/PCL conduits exhibited random distribution between −90° and 90°, whereas 96% of fibers in O-GO/PCL conduits were distributed between −15° and 15°. The distribution frequencies of fiber diameter for O-GO/PCL and R-GO/PCL are shown in Figure 2C and F. The average fiber diameter for both O-GO/PCL and R-GO/PCL nerve conduits was 941.84 ± 122.76 nm and 949.73 ± 130.15 nm, respectively. TEM image of the nanofiber membranes loaded with 0.5% GO showed homogenous, uniform, and non-agglomerated distribution of the particles inside the nanofibers (Figure 2G). Compared to PCL, which is a non-conductive material, the 4-point probe method results show that 0.5%GO/PCL nanocomposite scaffolds showed higher electrical conductivity up to 0.09 ± 0.01 S/m. The water contact angles were decreasing with the increasing of GO concentration (Supplemental Figure 2), which were 139.38° ± 2.03°, 130.77° ± 1.70°, 126.59° ± 1.59°, 123.55° ± 2.19° and 121.15° ± 1.97° for PCL, 0.1%O-GO/PCL, 0.3%O-GO/PCL, 0.5%O-GO/PCL and 1.0%O-GO/PCL, respectively (Figure 2H). With the addition of GO, the tensile stress of NGSs decreases to some extent. The tensile stresses of PCL, 0.1%GO/PCL, 0.3% GO/PCL, 0.5%GO/PCL and 1.0%GO/PCL scaffolds were 25.43 ± 2.35 MPa, 17.54 ± 3.24 MPa, 15.65 ± 2.77 MPa, 14.21 ± 2.20 MPa, and 11.57 ± 2.45 MPa, respectively (Figure 2I and J). The stretchability of PCL, 0.1% GO/PCL, 0.3% GO/PCL, 0.5% GO/PCL and 1.0% GO/PCL were 79.80 ± 5.09%, 69.32 ± 7.06%, 67.94 ± 5.61%, 67.61 ± 5.12%, and 59.95 ± 7.10% (Figure 2K). FTIR spectra of GO/PCL showed absorption bands at 1740 $cm^{-1}$ indicating carbonyl stretching. The bands appearing at 1290 $cm^{-1}$ and 1240 $cm^{-1}$ represented the C–O and C–C stretching bonds. The bands at 1236 and 1159 $cm^{-1}$ were comparable with the asymmetric C–O–C stretching bonds indicating characteristic absorption of PCL (Figure 2L).

## Cells Live/Dead Staining of the GO/PCL Scaffold

Primary SCs were used for biocompatibility testing instead of cell lines. Live/Dead staining indicated the survival of most cells after 3 days of culture on the scaffolds, with positive Calcein-AM (green) staining (Figure 3). Quantitative analysis revealed a survival rate of 81.68 ± 3.49% for cells in the 1.0% GO group, significantly lower than the other groups. Meanwhile, survival rates for the control, 0.1% GO, 0.3% GO, and 0.5% GO groups were 97.18 ± 1.51%, 96.04 ± 1.26%, 95.62 ± 1.52%, respectively, with no significant difference among them ($P > 0.05$). In order to fabricate a scaffold with maximum electroactive GO and negligible toxicity, a concentration of 0.5% GO was chosen for subsequent experiments.

## The O-GO/PCL Scaffold Accelerated Axonal Regeneration in vitro

DRG explants were cultured on O-GO/PCL, R-GO/PCL, O-PCL, and R-PCL scaffolds (Figure 4A–D). Axons from DRGs cultured on longitudinal O-GO/PCL and O-PCL scaffolds extended along the aligned nanofibers (Figure 4B and D). Axons showed no directional specificity for DRGs cultured on R-GO/PCL and R-PCL scaffolds (Figure 4A and C). Quantitative analysis revealed that about 84% and 81% of axons extended within ± 15° along aligned fibers in the O-GO/PCL and O-PCL groups (Figure 4F and H), while axons extended evenly at −180° to 180° in the R-GO/PCL and R-PCL groups (Figure 4E and G). The average axon length on the O-GO/PCL scaffold was 1054.88 ± 161.32 μm, significantly longer than R-GO/PCL (398.74 ± 84.10 μm, $P < 0.05$), O-PCL (573.81 ± 144.46 μm, $P < 0.05$), and R-PCL (291.95 ± 88.57 μm, $P < 0.05$) scaffolds (Figure 4I). To exclude the potential influence of larger explants that tend to exhibit larger outgrowths, the neurites/explant body ratio was also quantified (Figure 4J). Neurites/explant body ratio was 2.03 ± 0.35 in the O-GO/PCL group, significantly larger than R-GO/PCL (0.69 ± 0.14, $P < 0.05$), O-PCL (1.11 ± 0.26, $P < 0.05$), and R-PCL (0.50 ± 0.21, $P < 0.05$) groups.

## The O-GO/PCL Scaffold-Promoted Nerve Regeneration Involved a Series of Signaling Pathways Associated with Axon Attraction

As the volcano maps shown that there were 1121 downregulated and 779 upregulated DEGs between the O-GO/PCL and R-PCL groups (Figure 5A). The heat map of DEGs among O-GO/PCL, O-PCL, R-GO/PCL and R-PCL is presented in Figure 5B. The gene ontology analysis showed that up-regulated and down-regulated DEGs in O-GO/PCL group

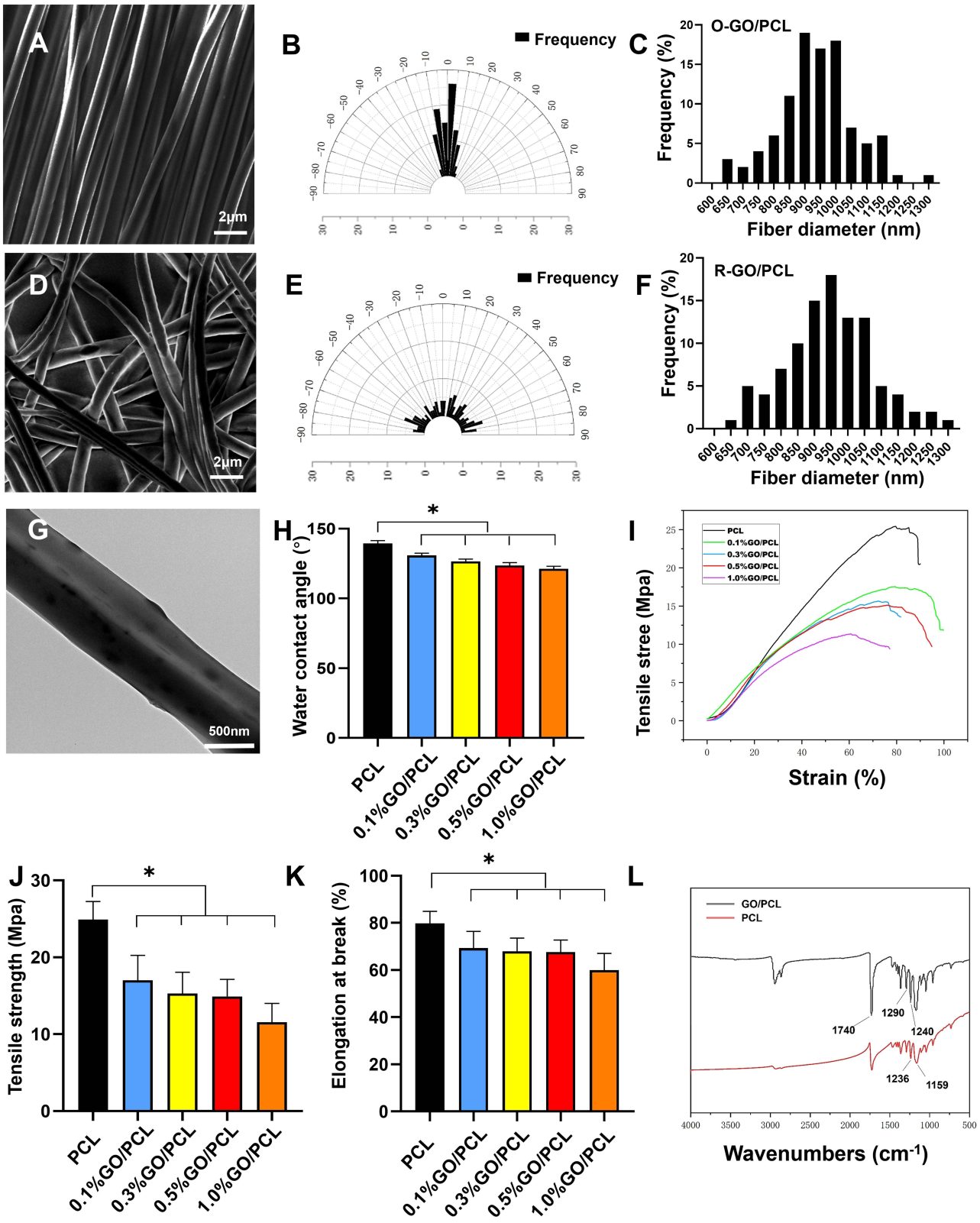


**Figure 2** Characterization of 0.5% GO/PCL scaffolds. SEM, TEM images and FTIR spectra.

**Notes**: (**A** and **D**) Fiber morphology at high magnification of O-GO/PCL and R-GO/PCL scaffolds. Distribution frequencies of fiber direction in (**B**) O-GO/PCL scaffold and (**E**) R-GO/PCL scaffold. Fiber diameter of (**C**) O-GO/PCL scaffold and (**F**) R-GO/PCL scaffold. (**G**) TEM of GO/PCL scaffold. (**H**) Water contact angle, (**I**) stress–strain curve, (**J**) tensile strength, (**K**) elongation at break and (**L**) FTIR spectra of GO/PCL scaffolds. *$P < 0.05$.

**Abbreviations**: O, Oriented; R, Random; GO, Graphene oxide; PCL, Polycaprolactone; TEM, Transmission electron microscopy; SEM, Scanning electron microscopy; FTIR, Fourier transform infrared.

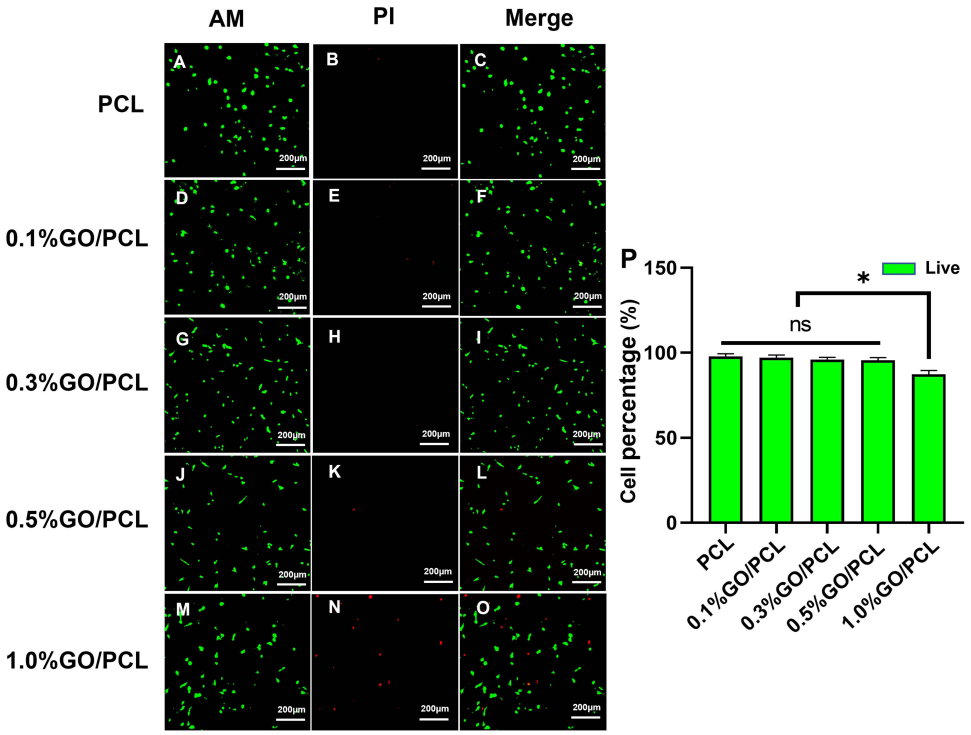


**Figure 3** Cell viability assay of Live/Dead cell staining.
**Notes**: (**A–C**) PCL (**D–F**) 0.1%GO/PCL, (**G–I**) 0.3%GO/PCL, (**J–L**) 0.5%GO/PCL, (**M–O**) 1 .0%GO/PCL. (**P**) Live cell counting. *p < 0.05.
**Abbreviations**: O, Oriented; R, Random; GO, Graphene oxide; PCL, Polycaprolactone.

enriched in gene ontology biological processes terms mainly related to ion transport, cell–cell adhesion, axonogenesis and extracellular matrix organization (Figure 5C). The DEGs between O-GO/PCL and R-PCL groups were enriched in 20 pathways by KEGG analysis (Figure 5D). These pathways are involved in neural regeneration, ion transport, and axon guidance. This molecular network suggests O-GO/PCL's potential mechanism for nerve regeneration, involving promoting ion transport, axon guidance and cell–cell interactions through excellent electrical conductivity of GO and highly oriented aligned topology.

## The O-GO/PCL Scaffold Promoted Nerve Regeneration in vivo

At 12 weeks post-surgery (Supplemental Figure 3A–D), immunostaining was performed on cross-sections of the middle nerve segments (Figure 6A–T). Immunostaining illustrates that a substantial number of axons (10,105.45 ± 990.92) regenerated within the middle of the O-GO/PCL graft, a significantly greater number than in the R-GO/PCL (4967.36 ± 265.54, P < 0.05), O-PCL (5980.68 ± 273.55, $P < 0.05$), and R-PCL (3194.44 ± 228.71, $P < 0.05$) groups (Figure 6U). Additionally, myelinated axons in the O-GO/PCL group (6512.82 ± 338.48, $P < 0.05$) displayed significant improvement compared to the R-GO/PCL (3406.97 ± 156.59, $P < 0.05$), O-PCL (4135.87 ± 345.93, $P < 0.05$), and R-PCL (2098.41 ± 297.29, $P < 0.05$) groups (Figure 6V).

Meanwhile, toluidine blue staining and TEM were employed to evaluate nerve regeneration that reached the distal segment (Figure 7A–O). The total count of myelinated fibers in the O-GO/PCL group was 4794.29 ± 506.22, significantly more than the numbers in the R-GO/PCL (2496.24 ± 247.78, $P < 0.05$), O-PCL (3010.34 ± 365.92, $P < 0.05$), and R-PCL (1450.20 ± 132.42, $P < 0.05$) groups (Figure 7P). Regarding axon diameter, the O-GO/PCL group (4.00 ± 0.25 μm, $P < 0.05$) displayed significantly larger to the R-GO/PCL (2.19 ± 0.17 μm, $P < 0.05$), O-PCL (2.55 ± 0.13 μm, $P < 0.05$), and R-PCL (1.48 ± 0.13 μm, $P < 0.05$) groups (Figure 7R). Furthermore, the myelin sheath thickness in the O-GO/PCL group (1.74 ± 0.16 μm, $P < 0.05$) was significantly improved compared to the R-GO/PCL (1.14 ± 0.08 μm, $P < 0.05$), O-PCL (1.36 ± 0.06 μm, $P < 0.05$), and R-PCL (0.41 ± 0.10 μm, $P < 0.05$) groups (Figure 7Q). The G-ratio data indicated that the myelination of

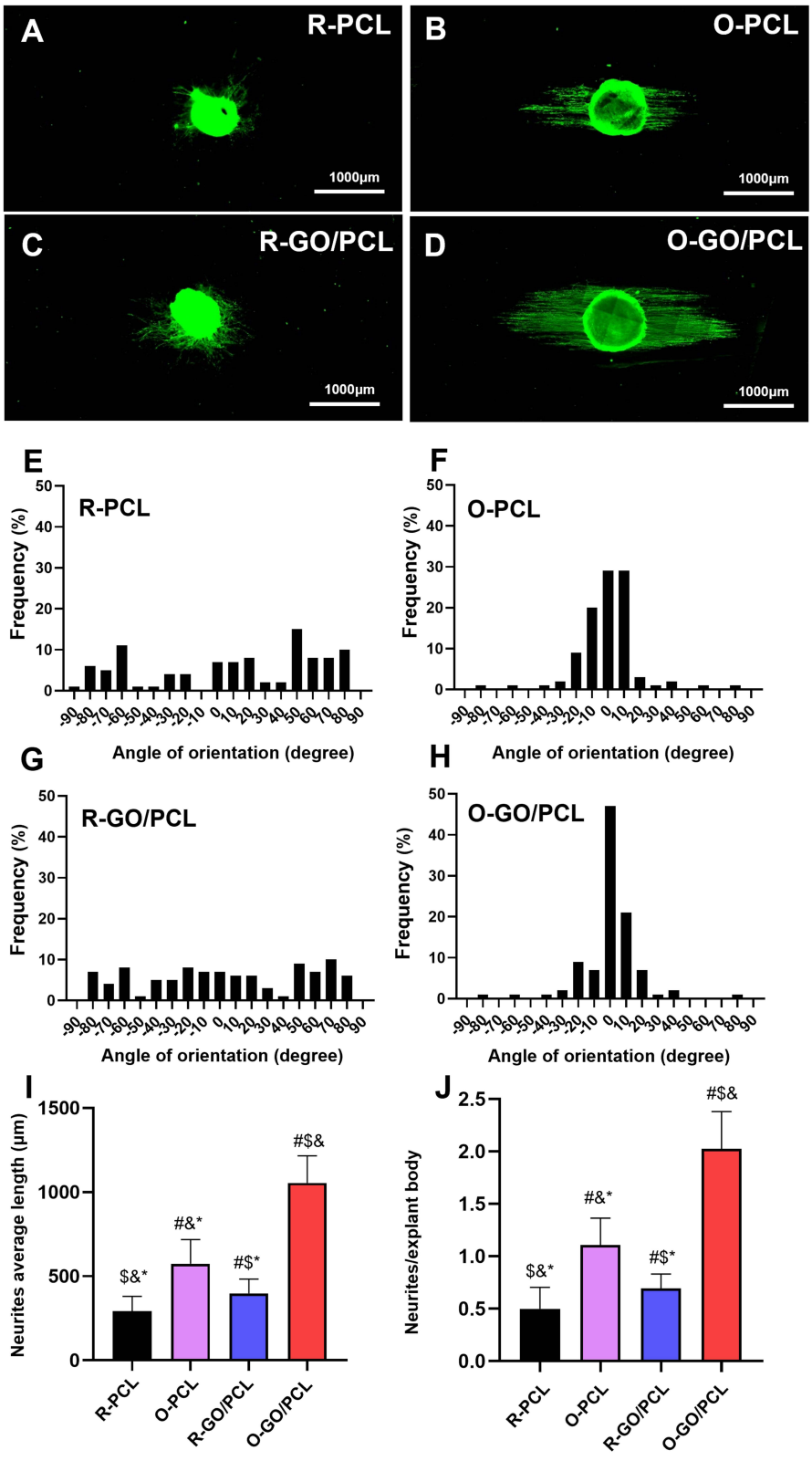


**Figure 4** DRG neurite outgrowth and orientation. DRGs growth on scaffolds for 72 h.

**Notes**: Extension angle of DRG axons in (**A**) R-PCL, (**B**) O-PCL, (**C**) R-GO/PCL, and (**D**) O-GO/PCL group. (**E–H**) Frequency distribution of four groups of axonal orientations. (**I**) Average axon length and (**J**) neurites/explant body ratio of four groups (n = 3 per group). $^{\#}p < 0.05$ for comparison with R-PCL group. $^{\$}p < 0.05$ for comparison with O-PCL group, $^{\&}p < 0.05$ for comparison with R-GO/PCL, $^{*}p < 0.05$ for comparison with O-GO/PCL.

**Abbreviations**: DRGs, Dorsal root ganglias; SC, Schwann cell.

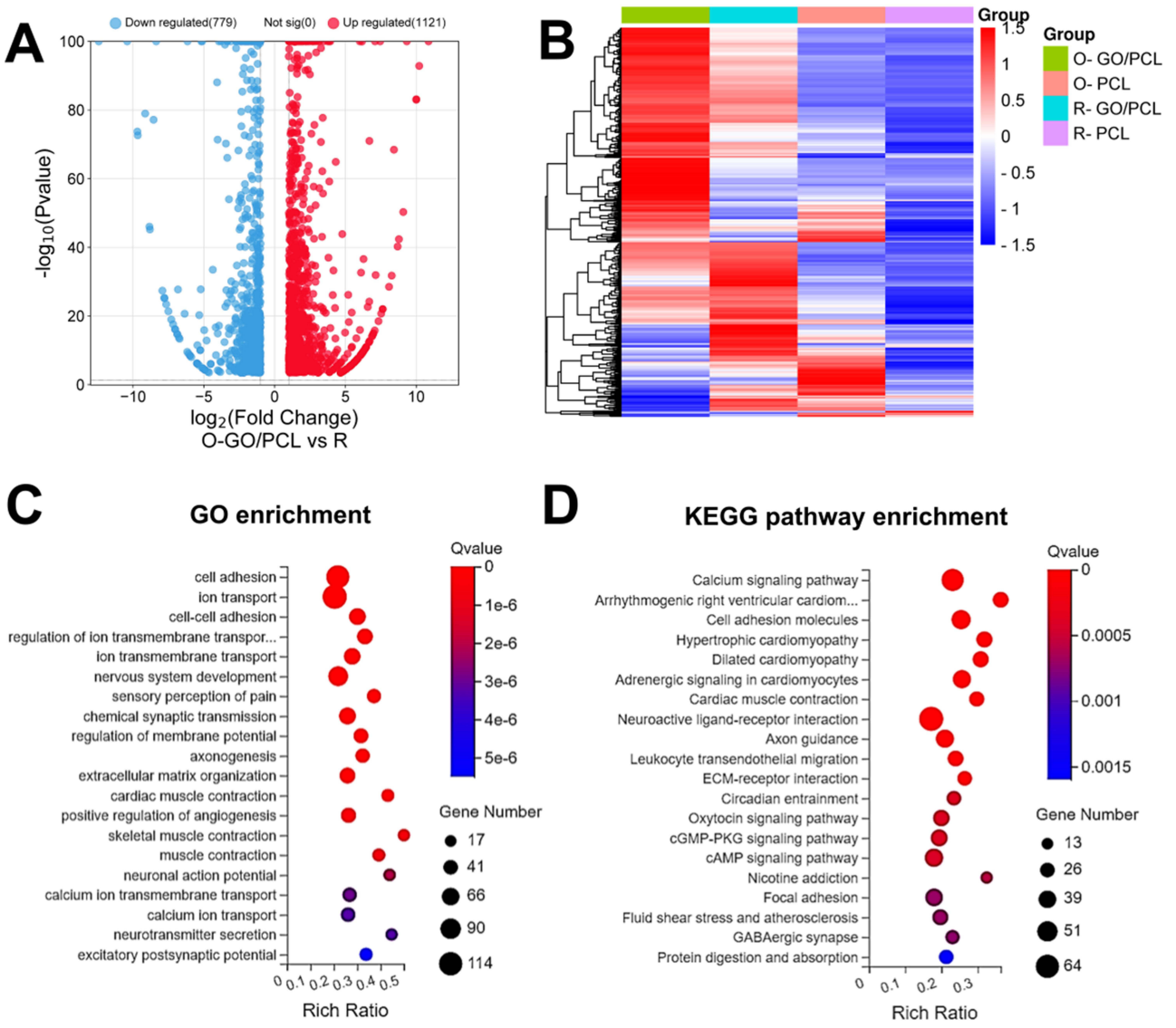


**Figure 5** Transcriptome profiles of nerve regeneration driven by O-GO/PCL scaffold.

**Notes**: (**A**) Volcano map of DEGs of DRG in O-GO/PCL versus R-PCL. Red dots indicate significantly upregulated DEGs and blue dots indicate significantly downregulated DEGs. (**B**) Heatmap of DEGs of DRG among R-PCL, O-PCL, R-GO/PCL and O-GO/PCL group. (**C**) Gene ontology terms enrichment. (**D**) KEGG pathway enrichment. (n = 3 per group).

**Abbreviations**: DEGs, Differentially expressed genes; DRGs, Dorsal root ganglias; O, Oriented; R, Random; GO, Graphene oxide; PCL, Polycaprolactone; GSEA, Gene set enrichment analysis.

regenerated axons in the O-GO/PCL group (0.63 ± 0.01, $P < 0.05$) was significantly superior to that in the R-GO/PCL (0.69 ± 0.03, $P < 0.05$), O-PCL (0.73 ± 0.02, $P < 0.05$), and R-PCL (0.82 ± 0.02, $P < 0.05$) groups (all $P < 0.05$) (Figure 7S).

## The O-GO/PCL Scaffold Improved Functional Recovery in vivo

At 12 weeks after surgery, the cross-sectional area of muscle fibers in the O-GO/PCL group was 894.06 ± 22.03 μm², significantly larger than those in the R-GO/PCL (660.12 ± 10.77 μm², $P < 0.05$), O-PCL (710.07 ± 9.02 μm², $P < 0.05$), and R-PCL (294.90 ± 29.46 μm², $P < 0.05$) groups (Figure 8A–F). The weight of the muscles in the O-GO/PCL group was 0.71 ± 0.01 of the contralateral side, which was significantly higher compared to the R-GO/PCL (0.56 ± 0.01, $P < 0.05$), O-PCL (0.58 ± 0.01, $P < 0.05$), and R-PCL (0.17 ± 0.01, $P < 0.05$) groups (Figure 8G).

The alleviation of muscle atrophy in the O-GO/PCL group exhibited a pattern consistent with the trend for functional recovery (Figure 9). Over time, animals in the ANT, O-GO/PCL, R-GO/PCL, O-PCL and R-PCL groups showed

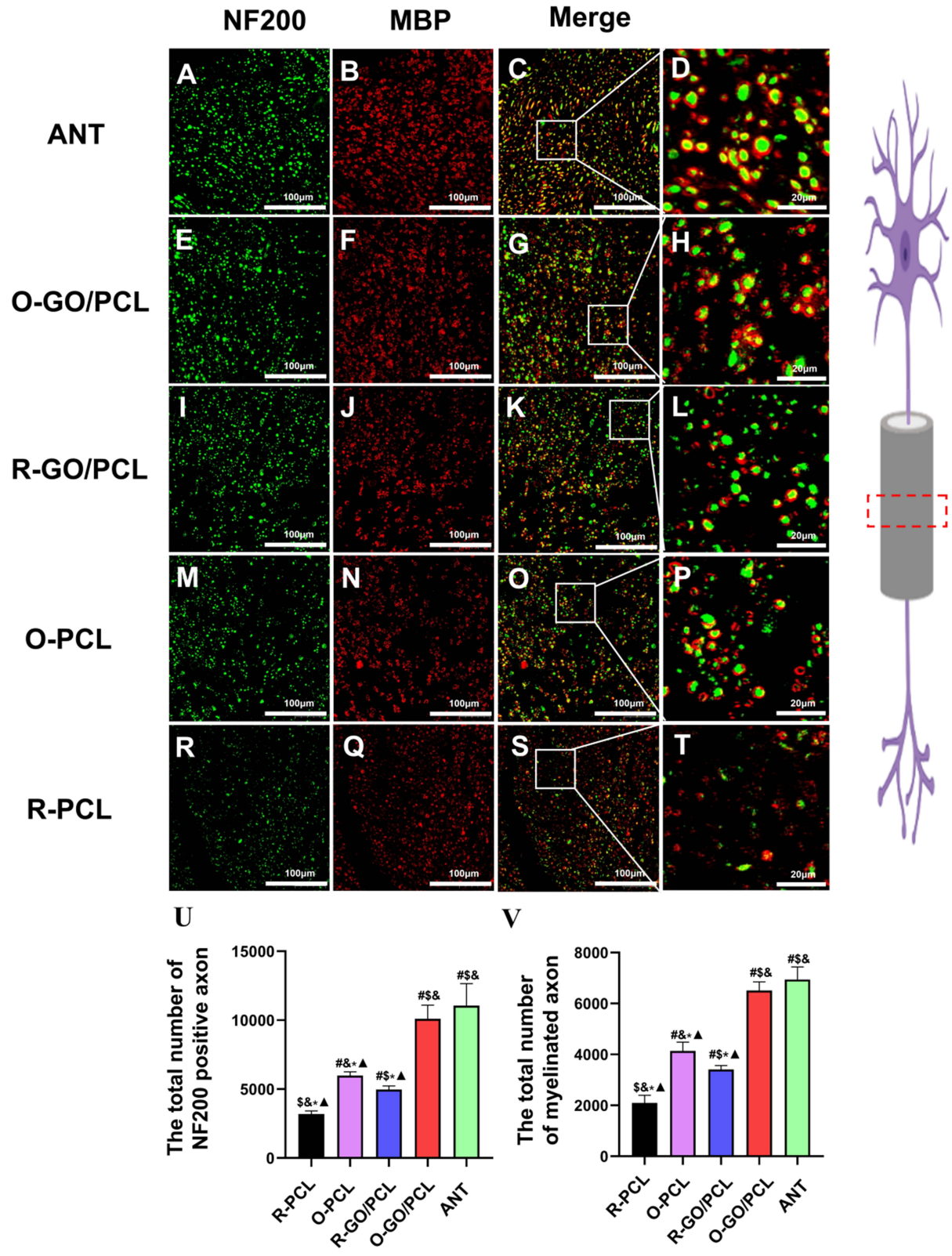


**Figure 6** Nerve regeneration at 12 weeks after surgery.

**Notes**: (**A-T**) Immunofluorescence staining of cross sections of the middle nerve segments at 12 weeks after surgery. Regenerated axons were labeled with NF200 (green), and myelin sheaths were labeled with MBP (red). (**U**) Quantification of the total number of NF200 positive axon and (**V**) the total number of myelinated axon (n=3 per group). $^{\#}p < 0.05$ for comparison with R-PCL group. $^{\$}p < 0.05$ for comparison with O-PCL group, $^{\&}p < 0.05$ for comparison with R-GO/PCL group, $^{*}p < 0.05$ for comparison with O-GO/PCL group, $^{\blacktriangle}p < 0.05$ for comparison with ANT group.

**Abbreviations**: O, Oriented; R, Random; GO, Graphene oxide; PCL, Polycaprolactone; ANT, Autogenous nerve transplantation.

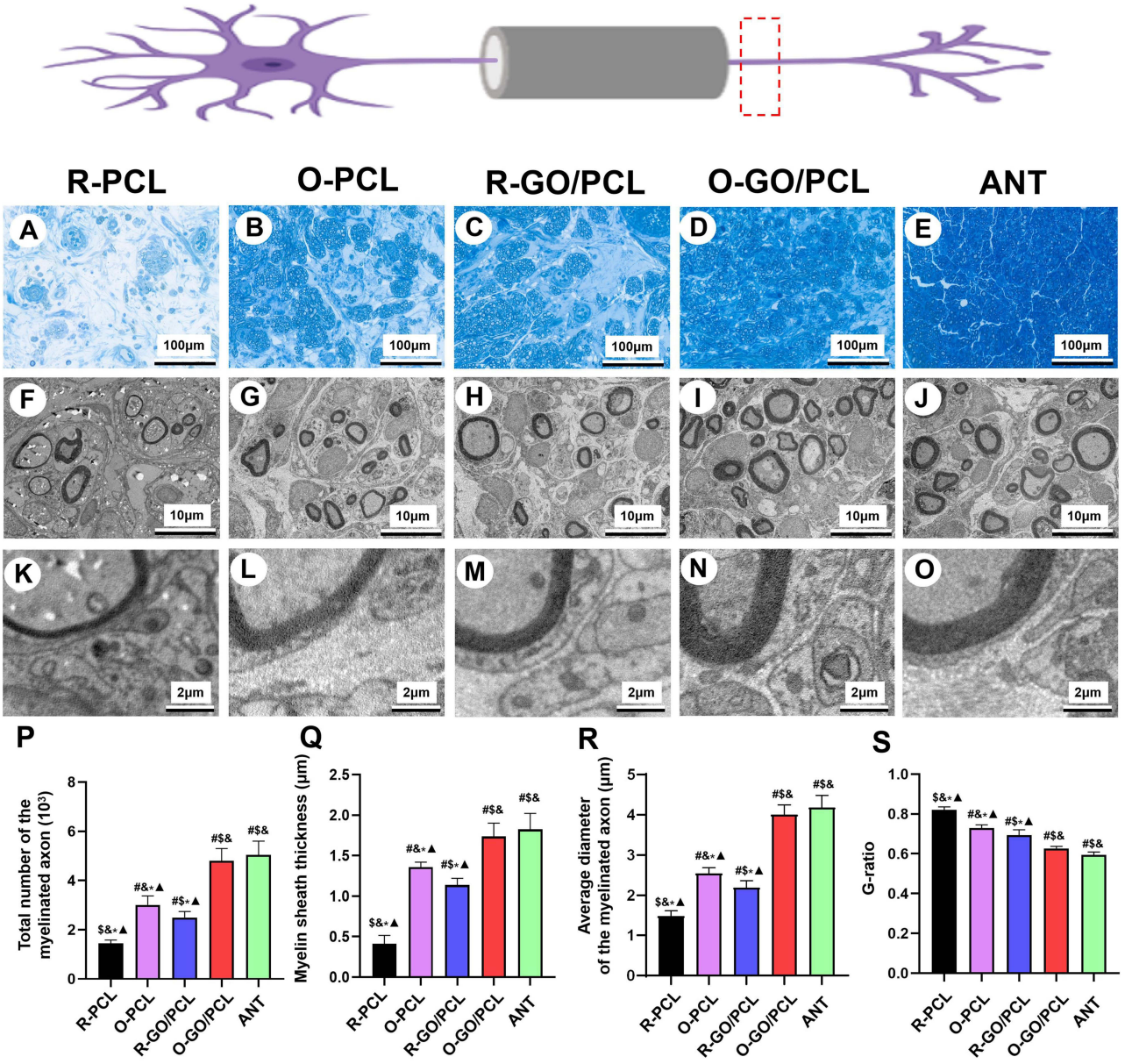


**Figure 7** Morphological appearances and morphometric assessments of regenerated nerves at 12 weeks following operation.
**Notes**: The regenerated axons in the (**A**) R-PCL, (**B**) O-PCL, (**C**) R-GO/PCL, (**D**) O-GO/PCL and (**E**) ANT groups were stained with toluidine blue. TEM micrographs of regenerated axons in (**F** and **K**) R-PCL, (**G** and **L**) O-PCL, (**H** and **M**) R-GO/PCL, (**I** and **N**) O-GO/PCL and (**J** and **O**) ANT groups. (**P**) Quantification of the total number of myelinated axons (**Q**) myelin sheath thickness, (**R**) average diameter of myelinated axons, and (**S**) G-ratios. $^{\#}p < 0.05$ for comparison with R-PCL group. $^{\$}p < 0.05$ for comparison with O-PCL group, $^{\&}p < 0.05$ for comparison with R-GO/PCL group, $^{*}p < 0.05$ for comparison with O-GO/PCL group, $^{\blacktriangle}p < 0.05$ for comparison with ANT group.
**Abbreviations**: O, Oriented; R, Random; GO, Graphene oxide; PCL, Polycaprolactone; ANT, Autogenous nerve transplantation; TEM, Transmission electron microscope.

improvements in the Sciatic Functional Index (SFI). In the mid-term of the experiment (at 6 weeks), the SFI in the O-GO/PCL group (−80.52 ± 2.60) demonstrated significant enhancement in comparison to the R-GO/PCL (−88.45 ± 1.96, $P < 0.05$), O-PCL (−84.87 ± 1.62, $P < 0.05$), and R-PCL (−96.61 ± 2.06, $P < 0.05$) groups. Upon completion of the experiment (at 12 weeks), the SFI in the O-GO/PCL group (-52.83 ± 3.66) also significant higher than that in the R-GO/PCL (-64.41 ± 2.78), O-PCL (-59.65 ± 3.07), R-PCL (-86.06 ± 1.68) groups. (Figure 9B).

## Discussion

Despite the inherent regenerative capability of the peripheral nervous system, commercially available tissue engineering nerve scaffolds for addressing nerve defects have yielded suboptimal therapeutic outcomes. Recent research has

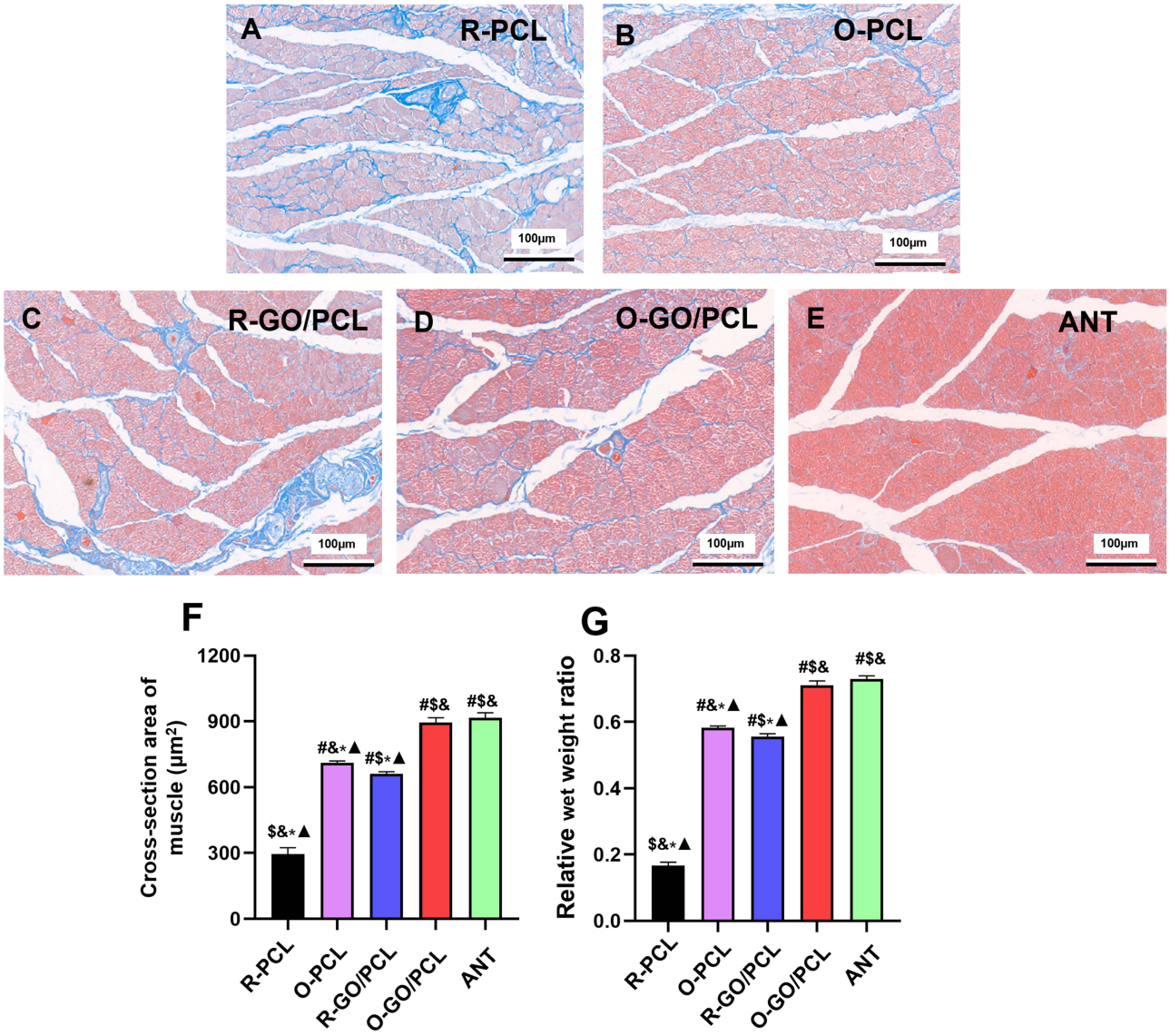


**Figure 8** Muscle atrophy analysis at 12 weeks following surgery.
**Notes**: Masson trichrome staining of the gastrocnemius muscles in the (**A**) R-PCL, (**B**) O-PCL, (**C**) R-GO/PCL, (**D**) O-GO/PCL and (**E**) ANT groups. (**F**) Cross-sectional area of muscle fibers. (**G**) Ratio of ipsilateral muscle wet weight to contralateral muscle wet weight. $^{\#}p < 0.05$ for comparison with R-PCL group. $^{\$}p < 0.05$ for comparison with O-PCL group, $^{\&}p < 0.05$ for comparison with R-GO/PCL group, $^{*}p < 0.05$ for comparison with O-GO/PCL group, $^{\blacktriangle}p < 0.05$ for comparison with ANT group.
**Abbreviations**: O, Oriented; R, Random; GO, Graphene oxide; PCL, Polycaprolactone; ANT, Autogenous nerve transplantation.

emphasized the significance of microstructure guidance and electroactivity in developing functional tissue engineering nerve scaffolds.[24,25] Herein, we employed a co-spinning technique to combine PCL with GO, resulting in nerve scaffolds characterized by highly oriented microstructures and electroactive GO. In vitro investigations corroborated the synergistic effect of electroactive GO and oriented microstructures in promoting nerve regeneration. Furthermore, mRNA-seq analysis revealed that O-GO/PCL scaffolds which combine topography and electroactive materials played pivotal roles in enhance nerve regeneration by upregulating genes associated with neural regeneration, encompassing ion transport, axon guidance and cell-cell interactions. Most importantly, in vivo experimentation demonstrated that the O-GO/PCL scaffold facilitated enhanced nerve regeneration towards distant targets, consequently promoting functional recovery. This study highlights the potential of O-GO/PCL scaffolds as an advanced therapeutic approach for peripheral nerve repair.

O-GO/PCL nanofiber neural scaffolds were fabricated by electrospinning and the microstructure was analyzed by SEM and TEM. We observed highly ordered nanofibers and homogeneously dispersed GO particles. As we expected, the water contact angle of the stent was significantly reduced after GO doping, while the electrical conductivity was significantly

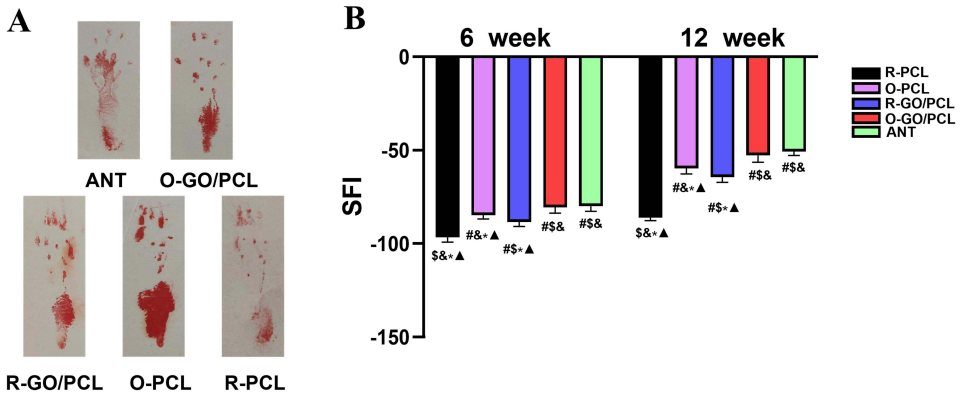


**Figure 9** Evaluation of functional recovery.
**Notes**: (**A**) Representative images of operative left footprints at 6 week and 12 weeks following nerve repair. (**B**) SFI measurements. $^{\#}p < 0.05$ for comparison with R-PCL group. $^{\$}p < 0.05$ for comparison with O-PCL group, $^{\&}p < 0.05$ for comparison with R-GO/PCL group, $^{*}p < 0.05$ for comparison with O-GO/PCL group, $^{\blacktriangle}p < 0.05$ for comparison with ANT group.
**Abbreviations**: O, Oriented; R, Random; GO, Graphene oxide; PCL, Polycaprolactone; ANT, Autogenous nerve transplantation.

improved. The drop in tensile strength is somewhat unexpected. This is in contrast to previous reports where tensile strength increases with the inclusion of a carbonaceous filler.[26] The reduction seen in this study is postulated to have been caused by disruption to the organization of polymer chains during scaffold preparation with the inclusion of GO sheets, compromising their (scaffold's) ability to dissipate stress. The intrinsic movement of polymer chains and their order inside a scaffold are also disrupted by filler particles, and this can reduce the stretchability of the scaffolds as seen above. The reduction in elongation is consistent with previous studies.[22]

Recent studies have underscored the influence of micropatterned surfaces on cell morphology and migration[27] and their ability to induce differentiation of neural stem cells (NSCs) and guide directed neurite growth from DRG neurons.[28] On the other hand, electroactive or functional materials have been reported to promote NSC proliferation, neuronal differentiation, and neurite elongation.[29,30] Given the crucial role of aligned microstructures and electroactivity in functional nerve scaffold development, various materials and strategies have been explored. For instance, Nazeri et al designed a multichannel nerve conduit employing longitudinally aligned laminin-coated poly(lactic-co-glycolic acid) (PLGA)/carbon nanotubes (CNT) nanofibers within the lumen and randomly oriented PCL nanofibers on the outer surface, leading to supported SC migration and axon extension.[31] Shang et al developed conductive composite films of polypyrrole (PPy) doped with sodium dodecyl benzenesulfonate and GO through electrochemical deposition of PPy nanoparticles on aligned poly-L-lactide (PLLA) fibers, thereby facilitating nerve tissue growth.[32] Zhang et al crafted conduits featuring surface-anchored GO nanosheets on micropatterned poly(D,L lactide-co-caprolactone).[15] In the present study, we co-spun PCL with GO to manufacture nerve scaffolds with a well-oriented microstructure and electroactive GO. The electrospinning technique endowed materials with an extensive surface area and a highly oriented microstructure conducive to cell attachment and directional migration. PCL was chosen for its FDA-approved biodegradability and excellent biocompatibility, making it suitable for various regenerative medicine applications, including vascular reconstruction and musculoskeletal tissue engineering. For endogenous electrical environments, GO held an advantage over materials like PPy, polyaniline (PANI), and poly(3,4-ethylenedioxythiophene) (PEDOT) due to its easy processability, strong affinity to specific biomolecules, and favorable interactions with cellular interfaces. Additionally, the straightforward approach of co-spinning PCL and GO to create an oriented GO/PCL hybrid scaffold and fabricating 3D nerve guidance structures rendered the O-GO/PCL scaffold a promising candidate for clinical translation into implantable scaffolds.

Existing studies underscore GO's concentration-dependent toxicity, increasing at higher concentrations.[33] Furthermore, the toxicity of GO exhibits significant variability across different cell types.[34,35] In this respect, Hu et al observed that lower concentrations of GO (20 μg/mL) had minimal impact on A549 cell viability compared to higher concentrations (85 μg/mL).[36] Conversely, Lv et al noted a 20% reduction in viability of the human neuroblastoma SH-SY5Y cell line after treatment with 100 mg/mL of GO for 96 hours.[37] Studies investigating GO-based materials' toxicity on neuronal cells have predominantly

used cell lines (eg, PC12, RSC96) in vitro. However, responses might differ between cell lines and in situ neural cells. Primary cells resemble organism-specific cellular characteristics more closely than cell lines, thus better guiding clinical applications. Our assessment of biocompatibility utilized primary SC cultures, revealing that GO/PCL scaffolds at a 0.5% concentration promoted peripheral nerve regeneration while circumventing overt cytotoxicity. This contrasts with prior findings suggesting minimal cytotoxicity at higher GO concentrations,[38] highlighting primary neural cells' potential tolerance to lower GO concentrations than cell lines and reinforces the importance of employing primary cells for comprehensive bioactivity assays.

Bioelectricity's concept and the presence of endogenous electric fields for tissue regeneration have been established for decades, playing a critical role in maintaining normal biological functions.[39] Neurons utilize endogenous electrical stimulation (ES) for impulse conduction—an active response generated by neurons. Consequently, transmitting endogenous ES represents an intrinsic neural capability. Moreover, the significance of conductive scaffolds in nerve repair lies in their direct contact with electrically active nerve tissues, enabling the delivery of peripheral nerve bioelectricity to expedite repair processes without external ES. Our study observed longitudinally extended axons of dorsal root ganglia along the fiber direction, with significantly longer axons in GO-based scaffolds than groups without GO. These findings align with earlier research indicating that micropatterns and GO synergistically enhance axon alignment and elongation.[15,19]

To evaluate O-GO/PCL scaffold effectiveness in promoting in vivo nerve regeneration, scaffolds were implanted to bridge 10mm rat sciatic nerve gaps. Immunostaining of graft midsections demonstrated superior axonal regeneration and remyelination in the O-GO/PCL group compared to the R-GO/PCL, O-PCL, and R-PCL groups. Additionally, cross-sectional analysis of distal nerve segments demonstrated significantly improved total myelinated fiber count and axon diameter in the O-GO/PCL group relative to the R-GO/PCL, O-PCL, and R-PCL groups. These findings were reinforced by muscle atrophy and SFI analyses, collectively substantiating the enhanced functional recovery of the O-GO/PCL group. Thus, our results validate that the scaffold's combination of electroactive GO and longitudinally oriented microstructure further enhances axonal regeneration and functional recovery in an in vivo context. Moreover, the safety of GO and its degradation products in vivo has been reported in previous studies. Mukherjee et al showed that GO was degraded by neutrophils in vivo, and its products were not significantly cytotoxic.[40] Interestingly, both in vitro and in vivo results showed that the O-PCL group were slightly better than those of the R-GO/PCL group, and such results may indicate that the effect of oriented topography in promoting peripheral nerve regeneration is more pronounced than that of using only conductive materials. It is noteworthy that the composite of oriented topology and electroactive materials showed a synergistical effect on promoting peripheral nerve regeneration.

The mechanism underlying the synergistic effect of GO and oriented microstructures in nerve regeneration remains largely unclear. To explore this, mRNA-seq was conducted to investigate mechanisms underlying nerve regeneration and axon attraction through electroactivity-driven neural regeneration. The analysis identified 20 KEGG pathways associated with topological structure and electroactivity-mediated neural regeneration. Some researches have shown that intracellular $Ca2^{+}$ level appears to affect cell viability, proliferation and differentiation in SCs and neuronal cells.[41–43] Wu et al showed that conductive materials decreased the intracellular $Ca2^{+}$ level, thereby inducing SCs' myelination.[30] In addition, Führmann et al showed the interactions of different cell types with each other within the scaffold appear to be influenced by the structure's longitudinally orientated micro-architecture to promote neural tissue repair.[44] Our results indicate that O-GO/PCL, a novel neural scaffold with a well-oriented microstructure and electroactive GO, may promote peripheral nerve regeneration by activating ion transport, axon guidance and cell–cell interactions. However, nerve regeneration is a process that includes many biological processes such as neuronal growth cone turning is a complex process in which actin-based motility is harnessed to produce persistent and directed microtubule advance.[45] A variety of adhesion molecules and other molecules that were enriched in our study may be involved in growth cone guidance, synaptogenesis, myelination, and axon growth. More studies are needed to address the roles of these identified and enriched differential genes in promoting electroactivity-driven neural regeneration and chemotactic axon growth.

## Conclusion

We introduced a straightforward co-spinning approach to create hybrid nanofibrous scaffolds with oriented microstructure and electroactive GO. The newly developed O-GO/PCL scaffold, combining electroactive and oriented physical cues, synergistically enhanced nerve regeneration and directional elongation in vitro. Furthermore, mRNA sequencing results indicated that the positive effect of O-GO/PCL scaffold on nerve regeneration might through activating ion transport, axon guidance and cell–cell interactions. Importantly, our in vivo studies validated that the amalgamation of oriented microstructures and electroactive GO

further elevated nerve regeneration and functional recovery. These outcomes underscore the potential of the O-GO/PCL scaffold, with its oriented microstructure and electroactive GO, as a promising candidate for peripheral nerve reconstruction.

## Acknowledgments

This work was supported by the National Natural Science Foundation of China (No. 81902213), the Health Commission of Hubei Province Scientific Research Project (No. WJ2021Q054), and the foundation from PLA (No. 18QNP054).

## Author Contributions

All authors made a significant contribution to the work reported, whether that is in the conception, study design, execution, acquisition of data, analysis and interpretation, or in all these areas; took part in drafting, revising or critically reviewing the article; gave final approval of the version to be published; have agreed on the journal to which the article has been submitted; and agree to be accountable for all aspects of the work.

## Disclosure

The authors declare no competing interest in this work.

## References

1. Pinho AC. Peripheral Nerve Regeneration: current Status and New Strategies Using Polymeric Materials. *Adv Healthc Mater*. 2016;5(21):2732–2744 doi:10.1002/adhm.201600236.
2. Vijayavenkataraman S. Nerve guide conduits for peripheral nerve injury repair: a review on design, materials and fabrication methods. *Acta Biomater*. 2020;106(54–69):1 doi:10.1016/j.actbio.2020.02.003.
3. Wang ML, Rivlin M, Graham JG, et al. Peripheral nerve injury, scarring, and recovery. *Connect Tissue Res*. 2019;60(1):3–9. doi:10.1080/03008207.2018.1489381
4. Du J, Chen H, Qing L, et al. Biomimetic neural scaffolds: a crucial step towards optimal peripheral nerve regeneration. *Biomater Sci*. 2018;6(6):1299–1311. doi:10.1039/C8BM00260F
5. Wangensteen KJ, Kalliainen LK. Collagen tube conduits in peripheral nerve repair: a retrospective analysis. *Hand*. 2010;5(3):273–277. doi:10.1007/s11552-009-9245-0
6. Thomsen L, Bellemere P, Loubersac T, et al. Treatment by collagen conduit of painful post-traumatic neuromas of the sensitive digital nerve: a retrospective study of 10 cases. *Chirurgie de la Main*. 2010;29(4):255–262. doi:10.1016/j.main.2010.07.004
7. Liu K, Yan L, Li R, et al. 3D Printed Personalized Nerve Guide Conduits for Precision Repair of Peripheral Nerve Defects. *Adv Sci*. 2022;9(12):e2103875. doi:10.1002/advs.202103875
8. Uz M, Büyüköz M, Sharma AD, et al. Gelatin-based 3D conduits for transdifferentiation of mesenchymal stem cells into Schwann cell-like phenotypes. *Acta Biomaterialia*. 2017;53:293–306. doi:10.1016/j.actbio.2017.02.018
9. Zhu J, Xiong Y, Zeng C, et al. Elastic chitosan conduits with multiple channels and well defined microstructure. *Int J Biol Macromol*. 2012;51(1–2):105–112. doi:10.1016/j.ijbiomac.2012.04.022
10. Al-hadeethi Y, Nagarajan A, Hanuman S, et al. Schwann cell-matrix coated PCL-MWCNT multifunctional nanofibrous scaffolds for neural regeneration. *RSC Adv*. 2023;13(2):1392–1401. doi:10.1039/D2RA05368C
11. Nune M, Bhat M, Nagarajan A. Design of ECM Functionalized Polycaprolactone Aligned Nanofibers for Peripheral Nerve Tissue Engineering. *J Med Biol Eng*. 2022;42(2):147–156. doi:10.1007/s40846-022-00699-3
12. Behtaj S, Ekberg JAK, St John JA, et al. Advances in Electrospun Nerve Guidance Conduits for Engineering Neural Regeneration. *Pharmaceutics*. 2022;14(2):219. doi:10.3390/pharmaceutics14020219
13. Nune M, Subramanian A, Krishnan UM, Kaimal SS, Sethuraman S. Self-assembling peptide nanostructures on aligned poly(lactide-co-glycolide) nanofibers for the functional regeneration of sciatic nerve. *Nanomedicine*. 2017;12(3):219–235. doi:10.2217/nnm-2016-0323
14. Zhang K, Zheng H, Liang S, et al. Aligned PLLA nanofibrous scaffolds coated with graphene oxide for promoting neural cell growth. *Acta Biomater*. 2016;37(131):131–142. doi:10.1016/j.actbio.2016.04.008
15. Zhang D, Yao Y, Duan Y, et al. Surface-Anchored Graphene Oxide Nanosheets on Cell-Scale Micropatterned Poly(d,l-lactide-co-caprolactone) Conduits Promote Peripheral Nerve Regeneration. *ACS Appl Mater Interfaces*. 2020;12(7):7915–7930. doi:10.1021/acsami.9b20321
16. Wang J, Zheng W, Chen L, et al. Enhancement of Schwann Cells Function Using Graphene-Oxide-Modified Nanofiber Scaffolds for Peripheral Nerve Regeneration. *ACS Biomater Sci Eng*. 2019;5(5):2444–2456. doi:10.1021/acsbiomaterials.8b01564
17. Qian Y, Song J, Zhao X, et al. 3D Fabrication with Integration Molding of a Graphene Oxide/Polycaprolactone Nanoscaffold for Neurite Regeneration and Angiogenesis. *Adv Sci*. 2018;5(4):1700499. doi:10.1002/advs.201700499
18. Wang J, Cheng Y, Wang H, et al. Biomimetic and hierarchical nerve conduits from multifunctional nanofibers for guided peripheral nerve regeneration. *Acta Biomaterialia*. 2020;117:180–191. doi:10.1016/j.actbio.2020.09.037
19. Liu X, Miller AL, Park S, et al. Functionalized Carbon Nanotube and Graphene Oxide Embedded Electrically Conductive Hydrogel Synergistically Stimulates Nerve Cell Differentiation. *ACS Appl Mater Interfaces*. 2017;9(17):14677–14690. doi:10.1021/acsami.7b02072
20. Li G, Zhao Y, Zhang L, et al. Preparation of graphene oxide/polyacrylamide composite hydrogel and its effect on Schwann cells attachment and proliferation. *Colloids Surf B Biointerfaces*. 2016;143:547–556. doi:10.1016/j.colsurfb.2016.03.079
21. Llewellyn SH, Faroni A, Iliut M, et al. Graphene Oxide Substrate Promotes Neurotrophic Factor Secretion and Survival of Human Schwann-Like Adipose Mesenchymal Stromal Cells. *Adv Biol*. 2021;5(4):e2000271. doi:10.1002/adbi.202000271

22. Nagarajan A, Rizwana N, Abraham M, et al. Polycaprolactone/graphene oxide/acellular matrix nanofibrous scaffolds with antioxidant and promyelinating features for the treatment of peripheral demyelinating diseases. *J Mater Sci*. 2023;34(10):49. doi:10.1007/s10856-023-06750-2
23. Varejo A, Meek MF, Ferreira AJ. Functional evaluation of peripheral nerve regeneration in the rat: walking track analysis. *J Neurosci Methods*. 2001;108(1):1–9 doi:10.1016/s0165-0270(01)00378-8.
24. Yao X, Qian Y, Fan C. Electroactive nanomaterials in the peripheral nerve regeneration. *J Mater Chem B*. 2021;9(35):6958–6972. doi:10.1039/D1TB00686J
25. Amaga TJ. Self-snapping hydrogel-based electroactive microchannels as nerve guidance conduits. *Mater Today Bio*. 2022;16:1 doi:10.1016/j.mtbio.2022.100437.
26. Fadil Y, Thickett SC, Agarwal V, et al. Synthesis of graphene-based polymeric nanocomposites using emulsion techniques. *Prog Polym Sci*. 2022;125:1 doi:10.1088/0031-8949/2012/T149/014068.
27. Zhang D, Xu S, Wu S, et al. Micropatterned poly(d, l -lactide- co -caprolactone) films entrapped with gelatin for promoting the alignment and directional migration of Schwann cells. *J Mater Chem B*. 2018;6(8):1226–1237. doi:10.1039/C7TB03073H
28. Lee JM, Kang WS, Lee KG, et al. Combinatorial biophysical cue sensor array for controlling neural stem cell fate. *Biosens Bioelectron*. 2020;156 (112125):112125. doi:10.1016/j.bios.2020.112125
29. Chao K-Y, Huang W-Y, Ho C-Y, et al. Biodegradable aniline-derived electroconductive film for the regulation of neural stem cell fate. *J Mater Chem B*. 2021;9(5):1325–1335. doi:10.1039/D0TB02171G
30. Wu Y, Wang L, Guo B, et al. Electroactive biodegradable polyurethane significantly enhanced Schwann cells myelin gene expression and neurotrophin secretion for peripheral nerve tissue engineering. *Biomaterials*. 2016;87(18):18–31. doi:10.1016/j.biomaterials.2016.02.010
31. Nazeri N, Derakhshan MA, Mansoori K, et al. Improvement of sciatic nerve regeneration by multichannel nanofibrous membrane-embedded electro-conductive conduits functionalized with laminin. *J Mater Sci Mater Med*. 2022;33(6):50. doi:10.1007/s10856-022-06669-0
32. Shang L, Huang Z, Pu X, et al. Preparation of Graphene Oxide-Doped Polypyrrole Composite Films with Stable Conductivity and Their Effect on the Elongation and Alignment of Neurite. *ACS Biomater Sci Eng*. 2019;5(3):1268–1278. doi:10.1021/acsbiomaterials.8b01326
33. Cebadero-Domínguez O, FerrÁndez-Gómez B, Sánchez-Ballester S, et al. In vitro toxicity evaluation of graphene oxide and reduced graphene oxide on Caco-2 cells. *Toxicol Rep*. 2022;9(1130):1130–1138. doi:10.1016/j.toxrep.2022.05.010
34. Yadav S, Singh Raman AP, Meena H, et al. An Update on Graphene Oxide: applications and Toxicity. *ACS Omega*. 2022;7(40):35387–35445. doi:10.1021/acsomega.2c03171
35. Li Y, Wang Y, Tu L, et al. Sub-Acute Toxicity Study of Graphene Oxide in the Sprague-Dawley Rat. *Int J Environ Res Public Health*. 2016;13 (11):1149. doi:10.3390/ijerph13111149
36. Hu W, Peng C, Luo W, et al. Graphene-based antibacterial paper. *ACS Nano*. 2010;7:4.
37. Lv M, Zhang Y, Liang L, et al. Effect of graphene oxide on undifferentiated and retinoic acid-differentiated SH-SY5Y cells line. *Nanoscale*. 2012;4 (13):3861. doi:10.1039/c2nr30407d
38. Rao F, Wang Y, Zhang D, et al. Aligned chitosan nanofiber hydrogel grafted with peptides mimicking bioactive brain-derived neurotrophic factor and vascular endothelial growth factor repair long-distance sciatic nerve defects in rats. *Theranostics*. 2020;10(4):1590–1603. doi:10.7150/thno.36272
39. Song B, Zhao M, Forrester J, et al. Nerve regeneration and wound healing are stimulated and directed by an endogenous electrical field in vivo. *J Cell Sci*. 2004;117(20):4681–4690. doi:10.1242/jcs.01341
40. Mukherjee SP, Gliga AR, Lazzaretto B, et al. Graphene oxide is degraded by neutrophils and the degradation products are non-genotoxic. *Nanoscale*. 2018;10(3):1180–1188. doi:10.1039/C7NR03552G
41. Subramanian A, Krishnan UM, Sethuraman S. Development of biomaterial scaffold for nerve tissue engineering: biomaterial mediated neural regeneration. *J Biomed Sci*. 2009;16(1). doi:10.1186/1423-0127-16-108
42. Huang J, Ye Z, Hu X, et al. Electrical stimulation induces calcium-dependent release of NGF from cultured Schwann cells. *Glia*. 2010;58 (5):622–631. doi:10.1002/glia.20951
43. Zhao X, Li P, Guo B, et al. Antibacterial and conductive injectable hydrogels based on quaternized chitosan-graft-polyaniline/oxidized dextran for tissue engineering. *Acta Biomaterialia*. 2015;26(236):236–248. doi:10.1016/j.actbio.2015.08.006
44. Führmann T, Hillen LM, Montzka K, et al. Cell–Cell interactions of human neural progenitor-derived astrocytes within a microstructured 3D-scaffold. *Biomaterials*. 2010;31(30):7705–7715. doi:10.1016/j.biomaterials.2010.06.060
45. Bradke F, Fawcett JW, Spira ME. Assembly of a new growth cone after axotomy: the precursor to axon regeneration. *Nat Rev Neurosci*. 2012;13 (3):183–193. doi:10.1038/nrn3176